Effects of post-weld heat treatment on the microstructural evolution and mechanical properties of dissimilar friction stir welded AA6061+SiCp/AA6061-O joint

Abstract

A research on the microstructure and mechanical properties of the dissimilar joint was carried out so as to understand the effects of post-weld heat treatment (PWHT) on microstructural evolution, microhardness, tensile and flexural properties of the dissimilar friction stir welded (FSWed) joint. The results showed that there is a sufficient and rather complicated material mixing in the nugget zone (NZ). After PWHT, the grains in the joint area except for the NZ demonstrated a grain refinement with more homogeneous and equiaxed grains. Fine and clustered SiC particles in the NZ are confirmed by scanning electron microscope (SEM). In addition, the microhardness values of nugget zones both in as-welded and PWHT condition exhibited a higher Vickers compared to that of AA6061-O. Furthermore, a mean tensile strength of 183.30 MPa that demonstrates a 52.22% increase in tensile strength is also observed in the transverse tensile tests subsequent to PWHT. Considering the three-point bending test results, it is explicit that an increase of 121.96% in the bending extension is obtained as there is no significant increase in maximum bending force after the PWHT.

Keywords
Friction Stir Welding, Metal Matrix Composites, Post-weld Heat Treatment, Mechanical Properties.

Nahit Oztoprak[a]*
Cınar Emine Yeni[b]
Binnur Goren Kiral[b]

[a] The Graduate School of Natural and Applied Sciences, Dokuz Eylul University, Izmir, Turkey, E-mail: nahit.oztoprak@deu.edu.tr

[b] Department of Mechanical Engineering, Dokuz Eylul University, Izmir, Turkey, E-mail: cinar.yeni@deu.edu.tr, binnur.goren@deu.edu.tr

*Corresponding author

1 INTRODUCTION

Metal-matrix composites (MMCs) are quite serviceable materials especially for aircraft, automotive and marine applications, where the weight reduction is important, when their properties of high strength to weight ratio is taken into consideration. MMCs are generally utilized for providing some significant advantages over conventional monolithic metals. These main advantages comprise high specific strength, elastic modulus, fatigue resistance, thermal conductivities, electric conductivities and abrasion resistance. On the other hand, MMCs have some drawbacks such as the properties of high density, high processing temperature or costly manufacturing process (Kaw 2006, Ceshini et al. 2007a, Cavaliere et al. 2008).

Recently, particle reinforced MMCs are increasingly finding their application in several industries such as automotive, aerospace, marine, electronics and sporting goods (Pirondi et al. 2008). Considering the global market trends, it is estimated that the MMC market will reach $431.1 million by 2020 at a compound annual growth rate (CAGR) of 5.7% from 2015 through 2020 (Shah 2016). Among MMCs, those based on aluminum alloy matrix have come continuously to the attention of various engineering fields of automotive, aerospace, marine, sports and recreation (Gopalakrishnan and Murugan 2011, Dinaharan and Murugan 2012a). Aluminum matrix composites (AMCs) have excellent specific stiffness, high strength to weight ratio, better wear resistance and superior fatigue properties in comparison with the corresponding monolithic alloys. AMCs also exhibit better high temperature properties (Kalaiselvan et al. 2014, Cioffi et al. 2013). In addition, Al-Mg-Si alloys including AA6061 have better strength, high corrosion resistance, better ductility and superior welding characteristics in comparison to other high-strength aluminum alloys (Elangovan et al. 2008, Ahmad and Bakar 2011, Ilangovan et al. 2015). Therefore, these alloys have widespread applications in marine frames, storage tanks, pipelines and aircraft parts. However, dissolution of Mg_2Si precipitates is an important problem in the heat affected zone that is affected only a thermal cycle (Elangovan et al. 2008).

When AMCs and monolithic alloys are practically used as the structural components, joining of these materials to provide good mechanical performance, obtaining cost-effective and promising assemblies is an important secondary process in the manufacturing of most structures. Therefore, sufficient joining of these materials are attractive in many engineering applications and can be acceptable to enhance mechanical properties by use of AMCs only at determined locations in a structure where necessary (Sharifitabar and Nami 2011, Guo et al. 2012). However, joining of these materials by conventional fusion welding processes may result in unfavorable effects such as chemical reactions between reinforcement-matrix material, presence of several inclusions and undesirable phases in matrix material (Lee et al. 2006, Feng et al. 2008, Wang et al. 2013, Prater et al. 2013). Friction stir welding (FSW) has become a unique welding technique suited for joining many hard to weld metals, especially high strength aluminum alloys due to its advantages provided as a solid-state joining method. FSW is also a strong candidate for welding of Mg-, Cu-, Ti-, Al-alloy matrix composites, some steels, stainless steels, thermoplastics and different material combinations, even though the technique was initially developed for Al-alloys (Çam 2011).

In recent years, several studies have been reported regarding the application of FSW to MMCs including aluminum alloy matrix AA6061. Prado et al. (2003) studied the amount of tool wear and wear rate at various traverse speeds in the FSW of AA6061/Al_2O_3/10p composite. Marzoli et al. (2006) evaluated the thermal and microstructural stability of aluminum matrix composite (AA6061/Al_2O_3/20p) subsequent to FSW and reported that a higher heat input is necessary at the beginning of the weld in order to obtain requisite plasticity. The effect of FSW on the microstructure evolution, tensile and low-cycle fatigue behavior of AA6061/Al_2O_3/20p metal matrix composite was also presented by the researchers (Ceshini et al. 2007b). Root et al. (2009) investigated the crystallographic texture and particle-matrix interaction during FSW in the AA6061/Al_2O_3/10p composite joints. Dinaharan and Murugan (2012b) carried out FSW of AA6061/ZrB_2 composites and studied the effect of FSW process on the microstructure, mechanical and wear properties of the joints. Besides all these, considerable work was also carried out on the application of friction stir processing (FSP), which is utilized for producing MMCs, so as to improve mechanical properties compared to the unreinforced alloys (Chen et al. 2015, Pantelis et al. 2016, Tabasi et al. 2016, Narimani et al. 2016). However, few papers can be found in the literature discussing the feasibility of dissimilar FSW between AMCs and monolithic alloys (Sharifitabar and Nami 2011, Guo et al. 2012). To the best knowledge of the authors, there is no study related to the influence of post-weld heat treatment (PWHT) on the microstructure and mechanical properties of dissimilar FSWed AA6061/SiC/20p composite and 6061-O aluminum alloy.

Considering the above fact, the primary objective of this study is to gain a better understanding of the effects of PWHT on the microstructural evolution, tensile and three-point bending properties, and hardness behavior of the dissimilar joint between AA6061/SiCp composite and AA6061-O fabricated by FSW. In the present work, AA6061/SiC/20p composite and AA6061-O are FSWed free of volumetric defects using a conical unthreaded tool of 4140 steel having HRC (Rockwell scale) 65. Then the microstructure and mechanical behavior of the dissimilar joint were scrutinized before and following the PWHT.

2 EXPERIMENTAL METHODS

Dissimilar sheet materials, namely 3.4 mm thick AA6061/SiC/20p composite and 3.2 mm thick AA6061-O were utilized during FSW process in this study. The composite used was fabricated by Materion (UK) via a powder metallurgy. Physical properties of the as-received composite material are given in Table 1 (SupremEX 620XF 2016). Chemical composition of the monolithic alloy is also shown in Table 2. The plates of size 300 mm x 120 mm were friction stir butt welded using a tool rotational speed of 1250 rpm, welding speed of 125 mm/min, tilt angle of 1°, and a penetration depth of 0.4 mm into the upper surface of the workpieces. The levels of each parameter were chosen by taking into consideration the results of preliminary experimental studies (Avettand-Fènoël and Simar 2016, Salih et al. 2015). In the current research, the monolithic alloy was fixed in the retreating side and single-pass welding process is performed. Temperature distribution in the weld line was also measured during the process by using the non-contact infrared thermometer (Fluke 576 CF) so as to provide a sound weld. The rotating welding tool with a shoulder having a diameter of 20 mm and an unthreaded pin of 5 mm diameter was manufactured from 4140 steel and then enhanced to a hardness of 65 HRC. Before FSW, surfaces of the plates were decontaminated from possible oxide films by a steel riffler. Thereafter, the joint was fabricated along the extrusion direction. General view of the welding process and dimensions of the fabricated tool are shown in Fig. 1.

The tensile properties of all specimens (as-welded and post-weld heat treated) were investigated in terms of tensile strength, percentage of elongation and also joint performance. Tensile tests were performed at room temperature at a constant speed of 1 mm/min using a Shimadzu AG-X (100 kN) Universal Testing Machine. Tensile test specimens were extracted from normal direction of the weld line according to ASTM: E8 and the test coupons were selected from different positions of the welding seam. At least three tensile tests were carried out for as-welded

Nahit Oztoprak et al.
Effects of post-weld heat treatment on the microstructural evolution and mechanical properties of dissimilar friction stir welded
AA6061+SiCp/AA6061-O joint

and post-weld heat treated (PWHTed) specimens so as to minimize the fudge factor. In addition, the Vickers micro-hardness profiles were also obtained across the mid-thickness of welds so as to evaluate the hardening effect of both FSW and PWHT processes. The measurements were performed with a loading of 100 g and a span of 0.5 mm. Moreover, three-point bending tests comprising only root test of the specimens were carried out according to the standard (EN ISO 5173) using same tensile testing machine with a crosshead speed of 2 mm/min and a span of 50 mm. Rectangular specimens having dimensions of 200 mm x 18 mm were tested before and after PWHT. Similarly, two bending tests are performed from each type.

The conventional metallographic methods (mounting, sanding, polishing, and etching) were utilized for the preparation of metallographic specimens. The characterization of the specimens before and after PWHT was performed through the Nikon Epiphot 200 inverted metallurgical microscope and the scanning electron microscope (SEM) of JEOL JSM-6060. The as-welded specimen was etched with Keller's reagent for 20 s and the specimen in the PWHTed condition was etched with $HF+HNO_3$ solution for 120 s in an attempt to obtain the macrostructures and also to evaluate the microstructures comprising of stir zone (SZ), thermomechanical affected zone (TMAZ), heat affected zone (HAZ) and the parent materials. In this work, a PWHT was carried out by way of solution heat treatment (530°C for 1 hour), followed by water quenching (rapid cooling in a water of 42°C) and finally artificial aging (178°C for 8 hour). Diagram in Fig. 2 describes the PWHT process. Besides that, Fig. 3 also demonstrates the dimensions of the tensile test specimens and the sampling schematic for joint characterization. Samples in the PWHTed conditions are coded as PWHT specimens in the other subsections.

Table 1: *Physical properties of AA6061/SiC/20p*

Density (g/cm³)	Elastic Modulus (GPa)	Specific Stiffness (GPa/g/cm³)	Poisson's Ratio	Solidus (°C)	Specific Heat Capacity (J/g/°C)
2.8	102	36	0.3	570	0.85

Table 2: *Chemical composition of 6061 aluminum alloy (wt.%)*

Material	Mg	Si	Fe	Cu	Cr	Zn	Mn	Ti
AA6061-O	1.1	0.68	0.6	0.3	0.19	0.14	0.09	0.03
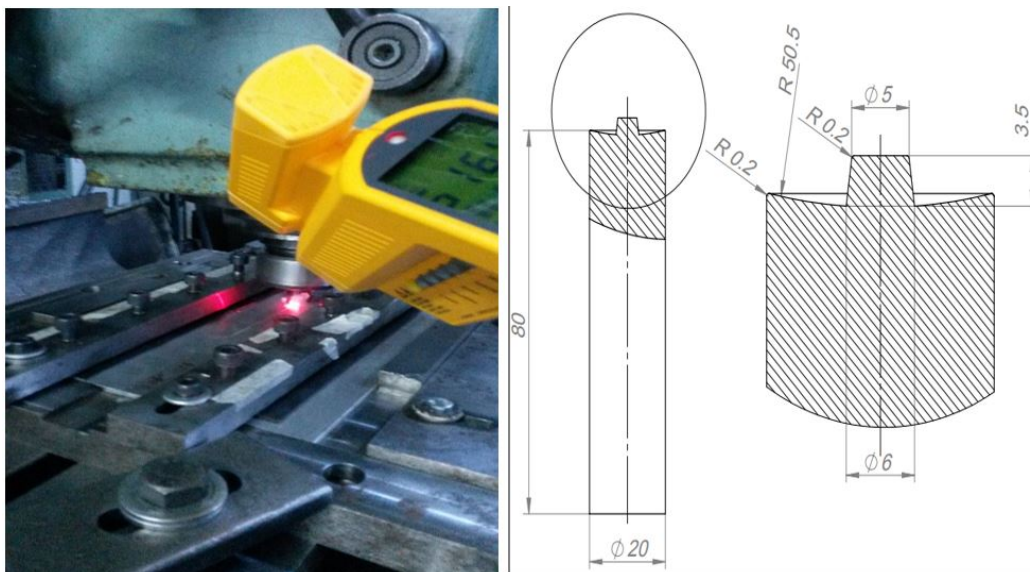
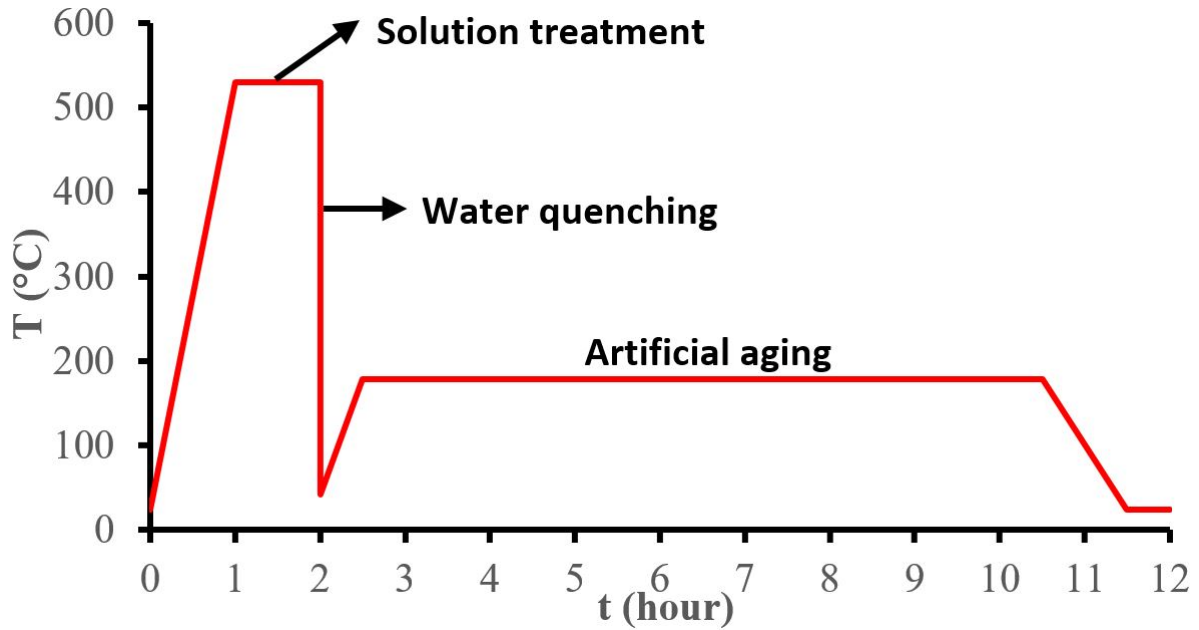**Figure 1:** *General view of (a) FSW process (b) fabricated tool dimensions*

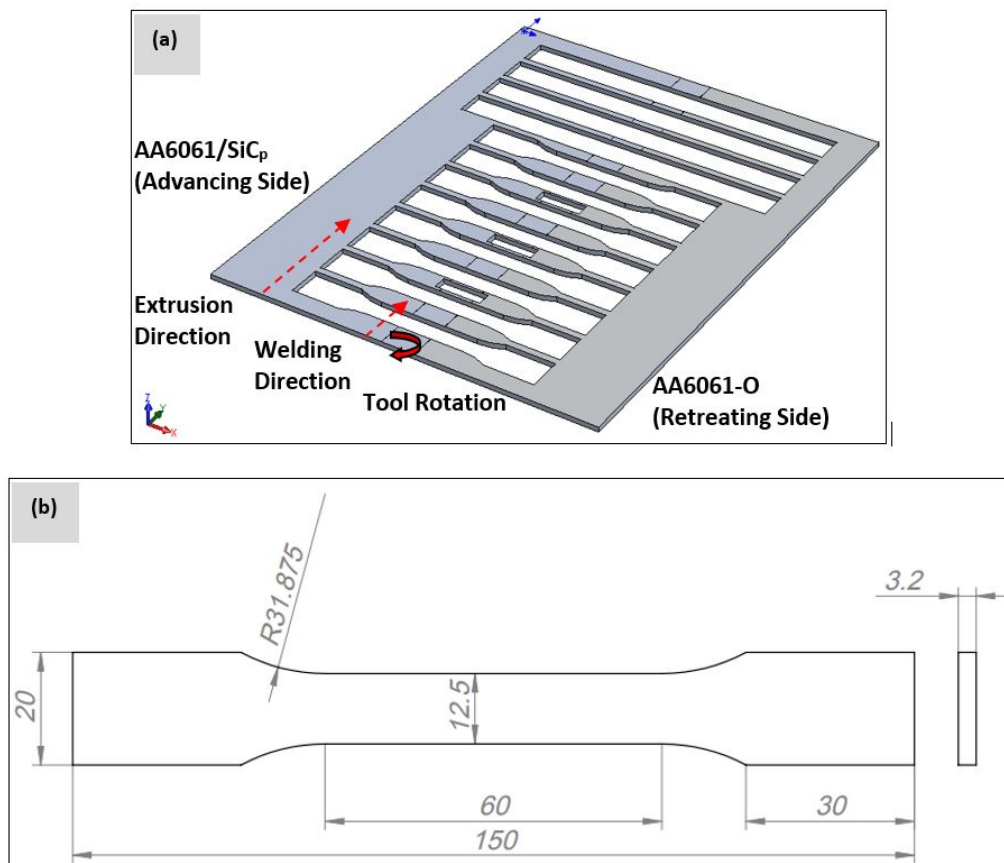**Figure 2:** *Schematic diagram of the PWHT process*

Figure 3: *(a) Sampling schematic of the joint (b) schematic illustration for the dimensions of tensile test specimens*

3 RESULTS AND DISCUSSION

3.1 Macrostructure and microstructure analysis

Fig. 4 reveals the macrostructures of dissimilar friction stir welded joint between AA6061/SiCp composite and 6061-O aluminum alloy before and after PWHT. It is evident from the figure that the accustomed fusion welding defects such as inclusions, apparent porosity, undesirable phases are not observed in the macrostructure figures. It is worth pointing out that the diversified thermomechanical histories of the joint create different zones including NZ, TMAZ and HAZ. A sufficient material mixing in the NZ is also achieved. In addition, the onion-ring structure can also be seen in Fig. 4a. On the other hand, an explicit interface between NZ and TMAZ is not observed with regards to the transition regions in both macrographs.
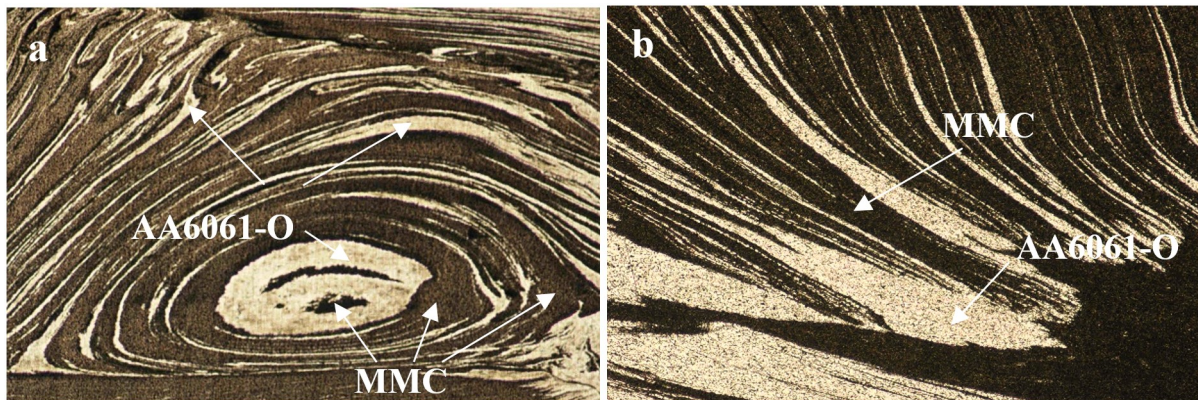

Figure 4: *Macrostructures of the joint (a) as-welded (b) after PWHT*

Fig. 5 reveals the effects of PWHT on the microstructure evolution of dissimilar friction stir welded joint in terms of the monolithic alloy side. Grain boundaries of the composite and the SiC particles cannot be observed through the instrument of optical microscope (OM) as the dimensions of aluminum powders in AA6061/SiC/20p (AMC620XF) are quite small. In addition, the average size of SiC particles used in the powder metallurgy process is about submicron. Therefore, only the particle distributions on MMC side are determined through the SEM before and subsequent to PWHT. This is because of the fact that the determination of grain size in particle reinforced composites is quite difficult due to the heavily dispersed SiC particles (Bahrami et al. 2014).

It was observed from Fig. 5a and Fig. 5e that the elongated dendritic microstructure of parent material disappeared after PWHT. In addition, grain refinement with more homogenous and equiaxed grains is realized. The average grain size of the sample after PWHT is determined to be about 30 μm. When the joint is subjected to PWHT, the elongated fibrous microstructure in HAZ is coarsened and the aspect ratio of the structure decreases. The TMAZ of as-welded joint also demonstrates significant change, deformed and elongated grains are observed in this region. The orientation of the grains in TMAZ owing to the material flow in consequence of the stirring effect of the tool can be seen in Fig. 5c and Fig. 5g. After PWHT, more equiaxed grains are reported. However, the grains having a higher average grain size (~35 μm) than those within TMAZ in as-welded specimen are also observed, locally (Fig. 5b). In the NZ, dynamically recrystallized and finer scale grains are formed due to the frictional and deformational heating. It should be noted that there is no significant difference in the grain size of these fine-equiaxed grains subsequent to PWHT. Besides all these, more precipitates can be seen explicitly in the joint area after PWHT.

By the way, it should be noted once again that the friction and plastic deformation play a significant role on the generated heat during the process. Besides, it is widely accepted that the microstructure and mechanical features of joint are considerably influenced by the generated heat (Serindag and Kiral 2017). It has been reported that the tool rotational speed has more influence on the frictional energy by comparison with other major FSW parameters such as the axial plunge force and welding speed (Aziz et al. 2016). Considering the heat generation rate based on the friction within the FSW process, some parameters such as the friction coefficient μ, probe radius r and angular velocity ω come into prominence. Regarding the temperature distribution in the weld zone, "V" shape temperature contour is generally observed (Chen and Kovacevic 2003). In other respects, the tool pin also makes a contribution to the generated heat through the friction on both threaded and vertical surfaces (Kovacevic et al. 2016). Herein, in order to assess the heat generation mechanisms in the modeling of FSW process, contact conditions such as the sticking, the sliding or partial sliding/sticking conditions can be thought as the probable contact states (Schmidt et al. 2004).
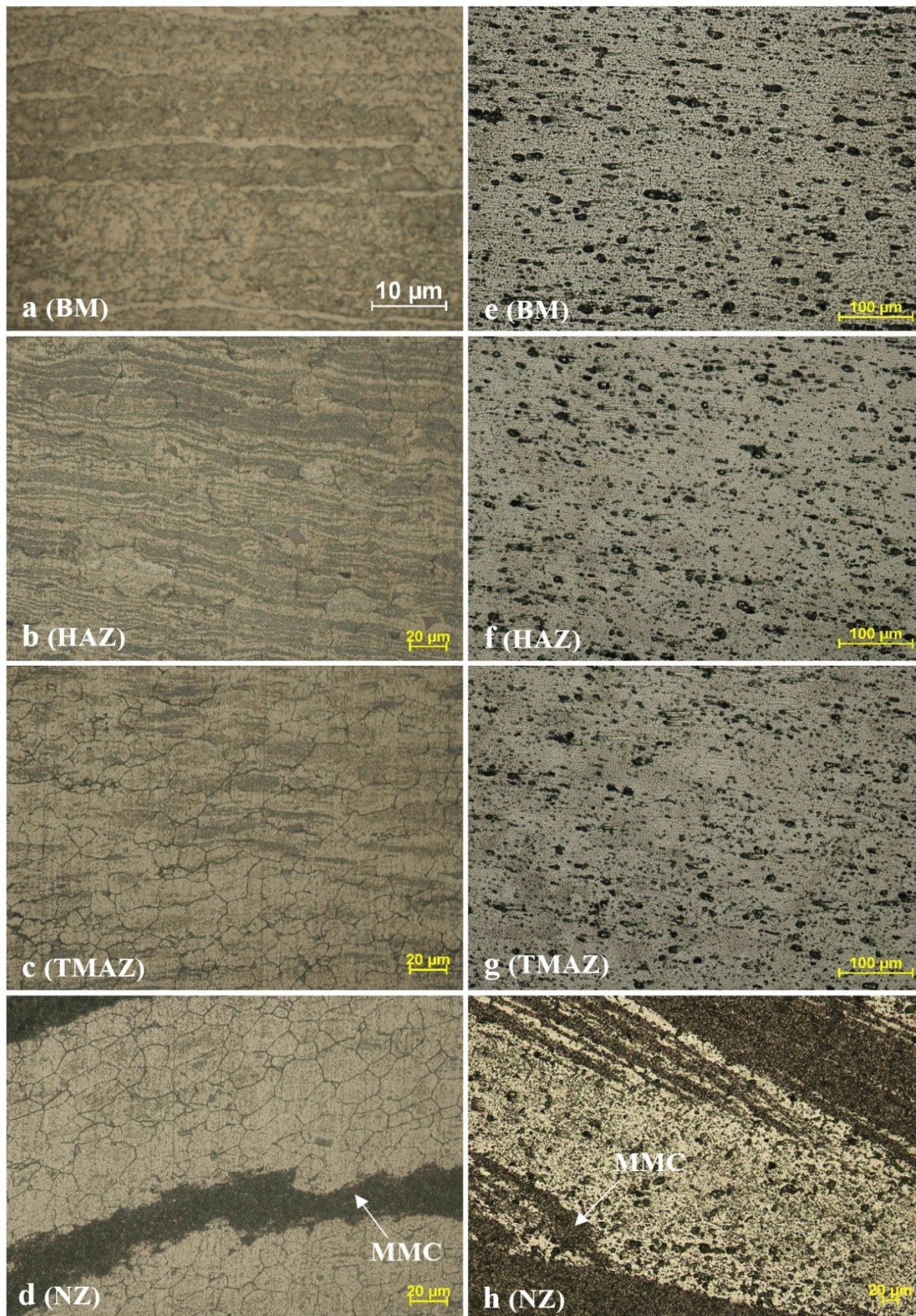
Figure 5: *Optical micrographs of as-welded (a-d) and PWHTed (e-h) specimens*

3.2 Dispersion of the particles

Energy dispersive x-ray (EDX) analysis in the composite side and EDX mapping in the NZ of the dissimilar joint are shown in Fig. 6 and Fig. 7, respectively. From Fig. 6, it is confirmed that the SiC particles are distributed in the aluminum matrix uniformly. In other words, there is no evidence for agglomeration of SiC reinforcements in the base composite matrix. Considering the element distributions in the NZ (Fig. 7), particle rich regions are seen locally though the SiC particles are distributed all over the matrix. It is also noteworthy to say that the NZ only comprises

the chemical composition of the workpieces. This evidences that there is no unfavorable new elements in the NZ owing to the tool wear especially. SEM micrographs of the particle dispersion in the joint area of the FSWed specimens before and after PWHT are shown in Fig. 8. According to this figure, it is observed that the size of coarse SiC particles in the BM shows an alteration from 0.7 µm to 2 µm. With the FSW process, shape and size of the particles in the joint area demonstrates a clear difference except for the HAZ. Fined and oriented SiC particles can be seen in the TMAZ. In the NZ, it is obvious that there are fractured SiC particles resulting from the abrasion through the welding tool and due to the attrition of SiC particles with each other (Sahraeinejad et al. 2015). In addition, FSW resulted in the clustering of SiC particles in the NZ. Moreover, the final shape of the SiC particles in the NZ are observed as more spherical compared to those in other joint regions. Fig. 8d shows the NZ of as-welded joint with the particle size of the base composite being about 0.5 µm. In addition, particle poor and particle rich regions can be seen in the figure. It should be noted that this is in tight agreement with the EDX mapping of NZ, as well. Fig. 8e-h exhibits the SEM micrographs of FSWed specimen after PWHT. With the PWHT, it is interesting to see that there is no remarkable difference in terms of the dispersion of SiC particles. Similar behavior is reported in the literature with regards to the distribution of the particles and also the matrix grain size (El-Sabbagh et al. 2013, Knowles et al. 2014). However, particle poor region in the NZ (Fig. 8h), which clearly demonstrates the particle-matrix interface, is reported in the specimen even as the number of particles has increased by comparison with the base composite.
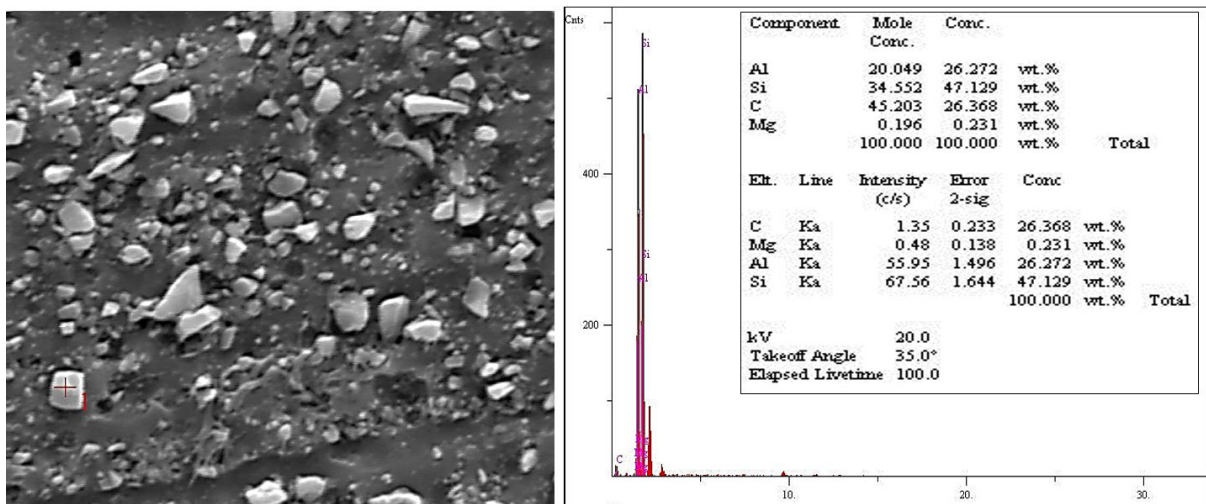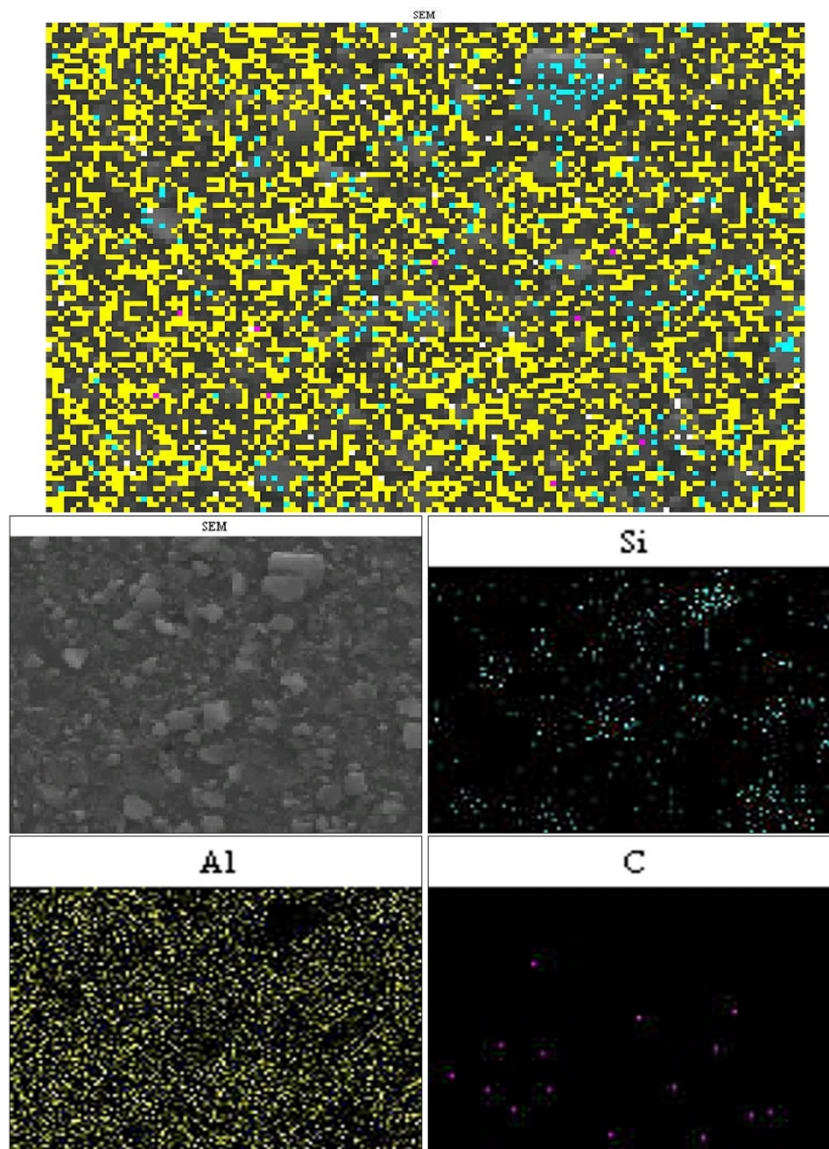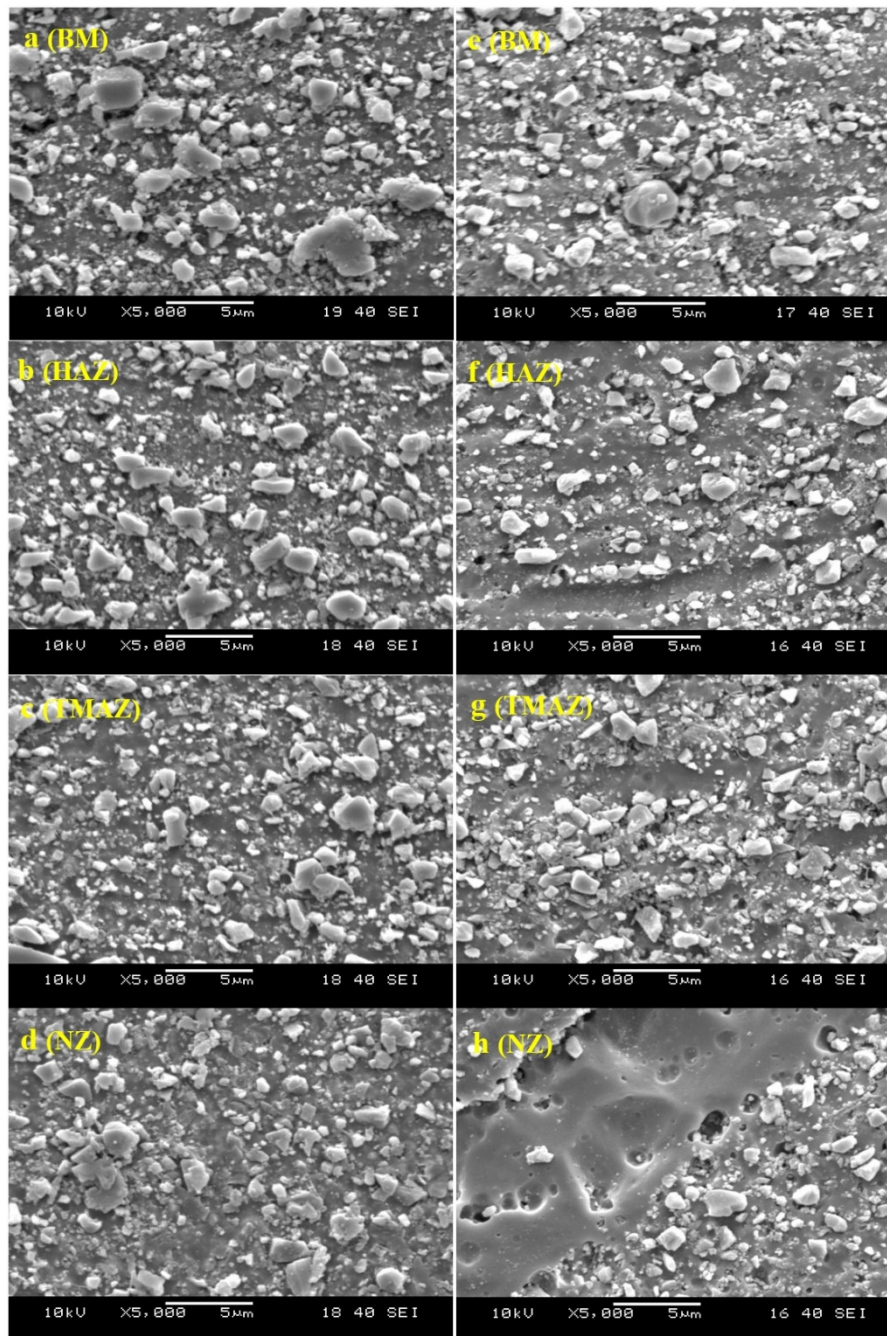

Figure 6: *EDX elemental analysis on AA6061/SiCp*

Figure 7: Mapping elemental analysis on the stir zone of as-welded specimen

Figure 8: SEM micrographs of as-welded (a-d) and PWHTed (e-h) specimens

3.3 Microhardness

The Vickers microhardness profiles are obtained across the mid-thickness of FSWed joints so as to evaluate the hardening effect of both FSW and PWHT processes. Hardness distributions of the joints are illustrated in Fig. 9. It is evident from the figure that there is an intricate mixing of workpieces. The complicated material patterns are thus viewed in the weld zone. Furthermore, the high energy input during FSW based upon the high tool penetration depth led to a wide joint area. As seen from the figure, the average hardness values of base materials for the monolithic alloy and the MMC are in the range of 40-44 HV and 144-158 HV, respectively. With the PWHT, an obvious increase in the microhardness at the base materials of both workpieces was observed. The maximum hardness values after PWHT on the AA6061/SiC/20p and AA6161-O are about 203 HV and 52 HV, respectively. In both conditions, the Vickers of stir zones are observed to be higher than that of the weaker material (AA6061-O). This obtained increment in hardness is associated with the microstructure evolution of the material that is in annealed condition. The decrement in the grain size and homogenous dispersion of the grains and precipitates due to the

high temperature and high plastic flow results in the given recovery. However, the same trends in the NZ are not observed when the hardness of AA6061/SiCp composite is considered. The main reason could probably be related to the change of material grain size and dispersion of precipitates locally due to the blend of the weaker material. Besides that, overaging and solution of metastable phases in the NZ may have an unfavorable effect in the hardness, as referred in the literature (Sharifitabar and Nami 2011, Kumar et al. 2015). When the figures are analyzed, it can be seen that there is an upward tendency in the microhardness from BM to NZ at the retreating side (RS) of as-welded specimen. In the HAZ of both sides, an explicit hardness increase can be seen compared to the base materials. The maximum hardness in TMAZ at RS is determined to be about 71.8 HV, while the hardness value in TMAZ at the advancing side (AS) is in the level of both NZ and the BM. In other words, there is no big difference between the hardness of NZ and BM at the composite side. After PWHT, it should be noticed that the hardness in HAZ at the RS is slightly lower than the hardness in HAZ at the side of AA6061-O in as-welded condition. At the same time, the hardness distribution within HAZ at the AS appears to be more disordered compared to that of RS. On the other hand, more homogenous hardness profile, which is in the level of BM, is obtained in TMAZ at the RS subsequent to PWHT. Moreover, a slight hardness loss was observed in TMAZ at the AS by comparison with the hardness of AA6061/SiCp composite. These hardness measurements clearly show that the PWHT can be used to enhance the hardness behavior of the dissimilar joint, though the process resulted in a complicated hardness distribution comprising sudden variances at the MMC side owing to the irregular dispersion of sub-micron reinforcing particles (Nikoo et al. 2016). Furthermore, it can be commented that the microhardness measurements are in good agreement with the microstructural characteristics obtained by OM.
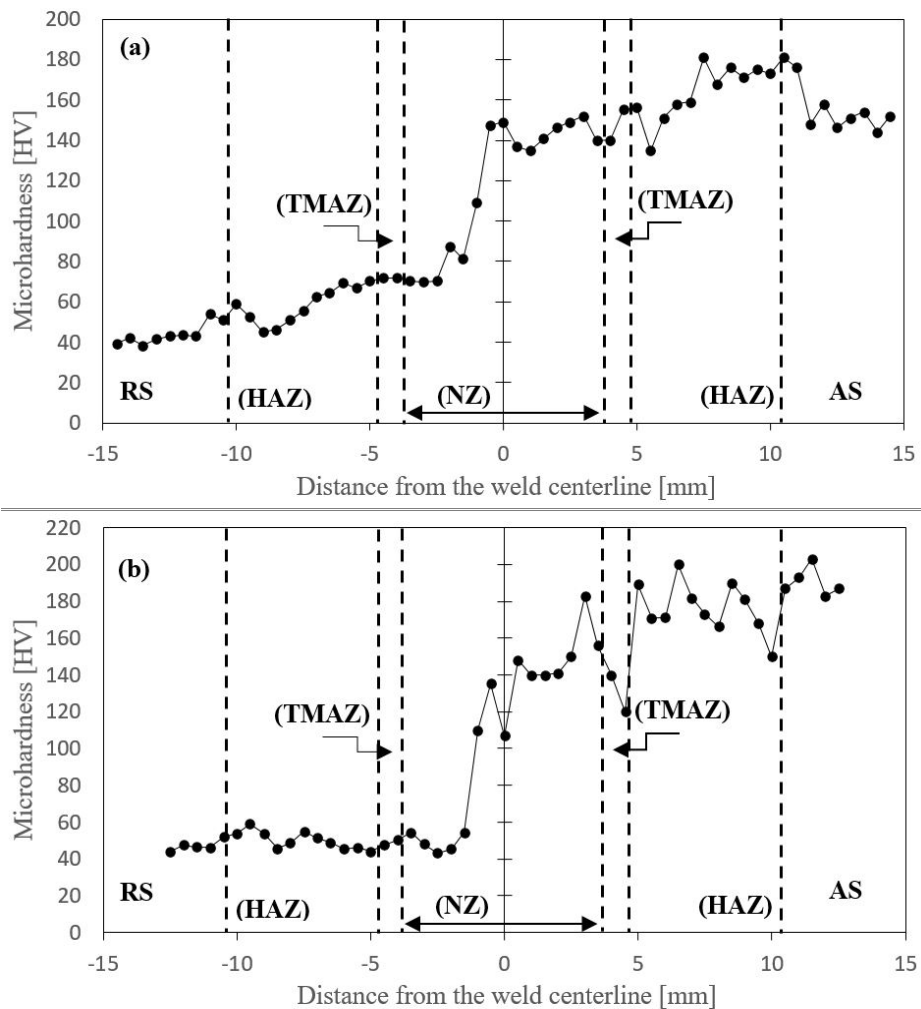
Figure 9: *Microhardness distributions of the joints in (a) as-welded and (b) PWHT condition*

3.4 Transverse tensile properties

The tensile strength and elongation (%) of unwelded AA6061/SiC$_p$ composite are obtained as 309.64 MPa and 5.62, respectively. The mechanical properties of the monolithic alloy in terms of the tensile strength and the elongation (P$_{ct}$) can be found in the Ref (İpekoğlu and Çam 2014). The engineering stress-strain curves of the as-welded tensile test specimens can be seen in Fig. 10. From the curves, it is observed that all specimens demonstrated a similar trend to those of AA6061-O parent material. The transverse tensile test results of as-welded specimens are also added to Table 3 for comparison. A higher mean tensile strength value, i.e., 120.74 MPa, is reported during the tests. The tensile test results also exhibited a joint efficiency of 103.64%, 103.29% and 103.17% in the FSWed specimens, respectively. These results mean that the appropriate selection of welding parameters and consequently obtaining a defect free weld resulted in a high joint-efficiency for the dissimilar joint between AA6061/SiC/20p composite and AA6061-O. In this study, joint efficiency is determined by dividing the ultimate tensile strength (UTS) of the dissimilar joint to that of the weaker material. In addition, all the test specimens fractured on the retreating side (AA6061-O) of the weld in the base material, as expected. This is in good agreement with the hardness measurements that demonstrates a significant hardness increase from BM to NZ. Failure positions of all specimens, which can be seen in Fig. 11, are also located away from the weld region. Thus, sound welding of the dissimilar workpieces is also proved. However, maximum failure strain of the specimens is about 9.25%, which represents 32.46% joint efficiency in terms of failure displacement. According to the results, it is worthwhile to mention that the successful FSW process can provide good performance in tensile strength, while reduces the elongation to failure in dissimilar joints between the AMC and the monolithic alloy.
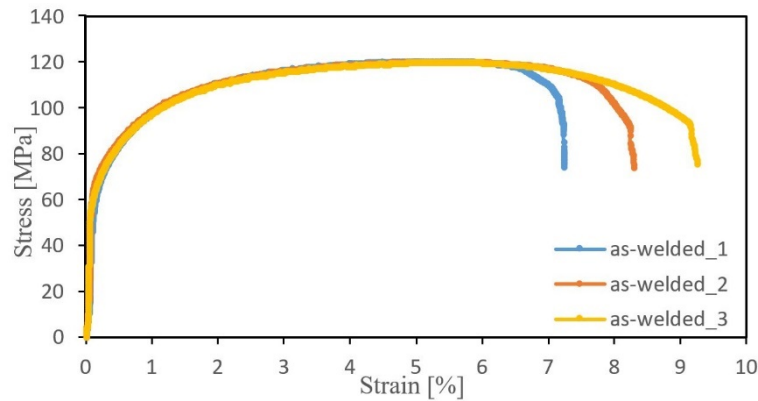

Figure 10: *Tensile behavior of the as-welded specimens*

Table 3: *Transverse tensile test results of as-welded specimens*

	Specimen_1	Specimen_2	Specimen_3
Tensile Strength [MPa]	120.74	120.33	120.19
Elongation (%)	7.24	8.29	9.25

Figure 11: *Fracture positions of the as-welded test specimens*

Nahit Oztoprak et al.
Effects of post-weld heat treatment on the microstructural evolution and mechanical properties of dissimilar friction stir welded
AA6061+SiCp/AA6061-O joint

The comparison of transverse tensile testing results including tensile strength and percentage of elongation of as-welded and PWHTed specimens are shown in Fig. 12. An average of three specimens is utilized for the calculation of tensile strength and elongation (%) values of both as-welded and PWHTed joints. It is clear from the figure that the PWHT effectively improves the tensile strength of the dissimilar joint while reduces the failure elongation. The tensile strength and elongation of PWHT joint are in the order of 183.30 MPa and 4.37%, respectively. It is evident from these results that there is a 52.22% increase in tensile strength after PWHT. This result clearly demonstrates that the microstructural modification owing to the dispersion of finer grains and precipitates in 6061 aluminum alloy uniformly improves the failure response of the dissimilar FSWed joint. On the other hand, PWHT also resulted in a decrease of 47.09% in the percentage of elongation. Considering the fact that the PWHT brings about a localized plasticity, this significant decrease can also be related to O-temper condition of the monolithic alloy.

In all specimens in PWHTed condition, fracture took place in the HAZ of welds at the RS. This is due to the slight microhardness loss close to the boundary between HAZ and the BM at the RS. Fracture positions of the PWHT specimens and SEM micrograph showing fracture surface of the tensile test specimen is demonstrated in Fig. 13. According to the SEM fractograph, the indications of ductile fracture mode including multitude dimples of various shapes are discovered in the fracture surface. The surface can also be characterized by tear ridges and shallow dimples that demonstrate inadequate toughness (Guo et al. 2017).
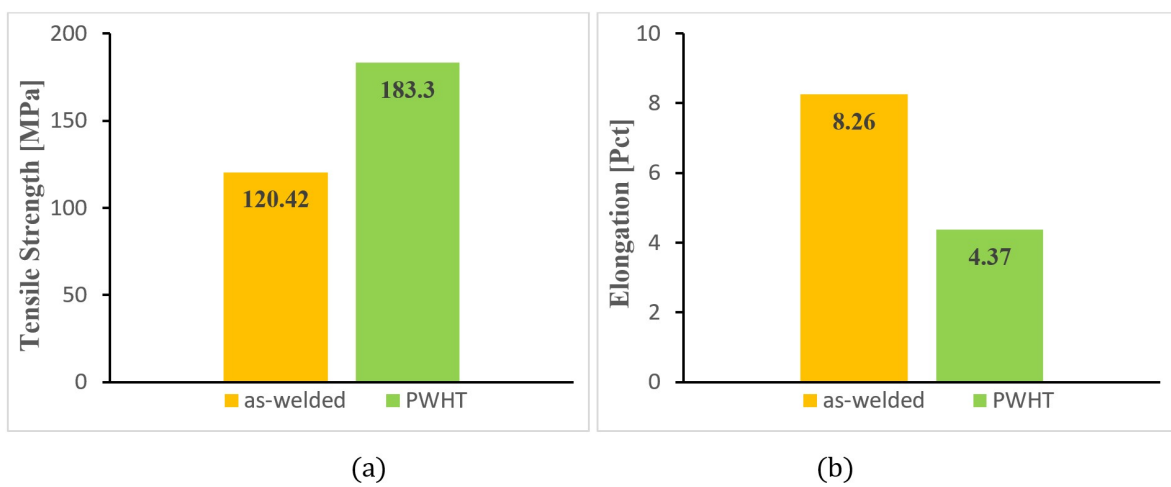

(a)   (b)

Figure 12: *Tensile behavior of the FSWed joints: (a) tensile strength (b) elongation [Pct]*

(a)   (b)

Figure 13: *PWHT specimens: (a) failure positions (b) SEM fractography*

3.5 Three-point bending properties

In this work, flexural properties of the FSWed specimens in both as-welded and PWHTed conditions are investigated by three-point bending tests. The tests are maintained until the FSWed specimens lose their load-carrying capacity and final bending shape is observed. Based on the experimental observations, no fracture is reported in all specimens during the bending tests.

Fig. 14 illustrates the comparison of bending force-extension behavior of the specimens before and after PWHT. From the figure, it can be inferred that the PWHT resulted in a slight increase in the maximum bending force. Maximum bending forces of the specimens after PWHT are in the order of 962.27 N and 1038.20 N, respectively. In addition, it is explicit from the results that the extension in three-point bending test shows a significant improvement subsequent to PWHT. An increase of 121.96% in bending extension is obtained in the PWHT specimens. Maximum bending extension is reported as 30.83 mm. Bending modulus of the specimens are also calculated during the tests. According to the results, modulus of 41.76 GPa and 81.76 GPa are obtained for as-welded and PWHT specimens, respectively. Thus, a substantial increase of 95.79% in bending modulus is provided after PWHT of the dissimilar FSWed joint.
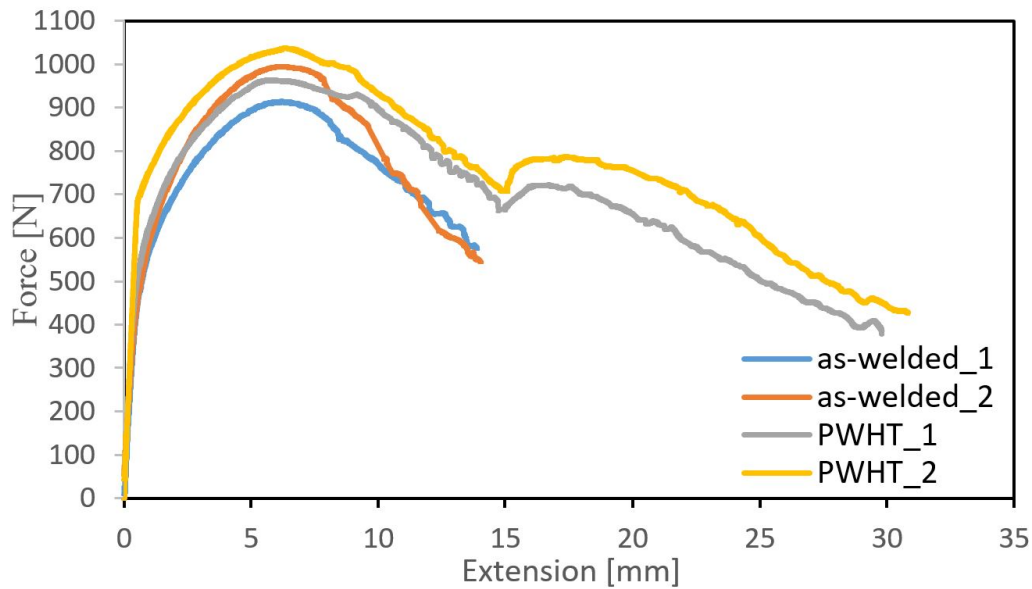
Figure 14: *Flexural behavior comparison of the welds before and after PWHT*

The bending angles before and after PWHT are shown in Fig. 15. It is evident from the figure that the bending angle increases subsequent to PWHT. This result means that a higher bending resistance is provided thanks to the PWHT. In addition, an L-shape is observed in as-welded specimens while the PWHT specimens take a U-shape during the three-point bending tests. As shown in the figure, there is another significant difference on the location of bending corners between different welds. Although bending in as-welded specimens takes place close to HAZ at the side of weaker monolithic alloy (AA6061-O), the location of bending corner is in the weld region for PWHT specimens. This can be associated with the improved mechanical properties of 6061 aluminum alloy after PWHT.
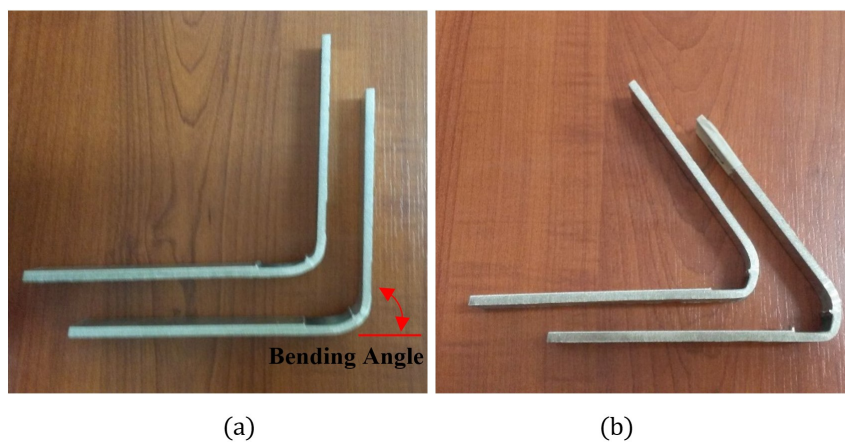
(a)   (b)

Figure 15: *Specimens after three-point bending tests: (a) as-welded (b) PWHTed*

4 CONCLUSIONS

In this paper, microstructure and mechanical behavior in terms of tensile, flexural and hardness properties of the dissimilar friction stir welded joint between AA6061/SiCp composite and AA6061-O were investigated experimentally. The effects of PWHT on these characteristics were also studied and discussed. Regarding the results, the following conclusions can be drawn:

a) After PWHT, few explicit differences are observed with regards to the fine-equiaxed recrystallized grains in the NZ.

b) Finer SiC particles are reported in the NZ with FSW. However, there is no big difference in the NZ with regards to the particle dispersion subsequent to PWHT.

c) The hardness values of stir zone in both as-welded and PWHTed condition are increased compared to that of the weaker material. The maximum hardness is found as 203 HV at the AS subsequent to PWHT.

d) FSW results in a maximum joint efficiency of 103.64% in terms of the transverse tensile strength. However, the tensile test results demonstrate a 32.46% maximum joint efficiency in terms of failure displacement, though the process exhibits a 64.59% increment compared to the elongation properties of AA6061/SiC$_p$ composite.

e) A mean transverse tensile strength of 183.30 MPa that demonstrates a 52.22% increase in the strength is also observed with the PWHT. On the other hand, ductility of the dissimilar joint declines with the applied PWHT.

f) In as-welded condition, fracture takes place away from the weld region at the RS of all specimens while tensile failure occurs within HAZ at the RS subsequent to PWHT.

g) Even though there is no explicit increase in the maximum bending force, PWHT improves the bending extension and the bending modulus in the order of 121.96% and 95.79%, respectively.

As a result, there is an explicit need for more efforts to understand the effects of various welding parameters such as the tilt angle, tool penetration depth, axial force, material position and so forth on the microstructural evolution and mechanical properties of dissimilar joints, even though this research presents a well-rounded experimental investigation on the dissimilar butt joint between the AMC and the monolithic alloy fabricated by using FSW. Besides, the applications of FSW of dissimilar AMCs are still limited and extensive work is also needed to evaluate the feasibility of FSW between AMCs and other promising materials such as titanium and magnesium alloys in many engineering applications.

References

Ahmad, R., Bakar, M. A., (2011). Effect of a post-weld heat treatment on the mechanical and microstructure properties of AA6061 joints welded by the gas metal arc welding cold metal transfer method. Materials & Design 32:5120-5126. doi: 10.1016/j.matdes.2011.06.007

Avettand-Fènoël, M-N., Simar, A., (2016). A review about friction stir welding of metal matrix composites. Materials Characterization 120:1-17. doi: 10.1016/j.matchar.2016.07.010

Aziz, S.B., Dewan, M.W., Huggett, D.J., Wahab, M.A., Okeil, A.M., Liao, T.W., (2016). Impact of Friction Stir Welding (FSW) Process Parameters on Thermal Modeling and Heat Generation of Aluminum Alloy Joints. Acta Metallurgica Sinica (English Letters) 29(9):869-883. https://doi.org/10.1007/s40195-016-0466-2

Bahrami, M., Givi, M. K. B., Dehghani, K., Parvin, N., (2014). On the role of pin geometry in microstructure and mechanical properties of AA7075/SiC nano-composite fabricated by friction stir welding technique. Materials & Design 53:519-527. doi: 10.1016/j.matdes.2013.07.049

Cavaliere, P., Rossi, G.L., Di Sante, R., Moretti, M., (2008). Thermoelasticity for the evaluation of fatigue behaviour of 7005/Al$_2$O$_3$/10p metal matrix composite sheets joined by FSW. International Journal of Fatigue 30:198-206. doi: 10.1016/j.ijfatigue.2007.01.021

Ceshini, L., Boromei, I., Minak, G., Morri, A., Tarterini, F., (2007a). Effect of friciton stir welding on microstructure, tensile and fatigue properties of the AA7005/10 vol.% Al$_2$O$_3$ composite. Composites Science and Technology 67:605-615. doi: 10.1016/j.compscitech.2006.07.029

Ceshini, L., Boromei, I., Minak, G., Morri, A., Tarterini, F., (2007b). Microstructure, tensile and fatigue properties of AA6061/20 vol.%Al$_2$O$_{3p}$ friction stir welded joints. Composites: Part A 38:1200-1210. doi: 10.1016/j.compositesa.2006.06.009

Chen, C.M., Kovacevic, R., (2003). Finite element modeling of friction stir welding-thermal and thermomechanical analysis. International Journal of Machine Tools & Manufacture 43:1319-1326. doi:10.1016/S0890-6955(03)00158-5

Chen, Z., Li, J., Borbely, A., Ji, G., Zhong, S. Y., Wu, Y., Wang, M. L., Wang, H. W., (2015). The effects of nanosized particles on microstructural evolution of an in-situ TiB2/6063Al composite produced by friction stir processing. Materials & Design 88:999-1007. doi: 10.1016/j.matdes.2015.09.127

Cioffi, F., Fernandez, R., Gesto, D., Rey, P., Verdera, D., Doncel, G. G., (2013). Friction stir welding of thick plates of aluminum alloy matrix composite with a high volume fraction of ceramic reinforcement. Composites: Part A 54:117-123. doi: 10.1016/j.compositesa.2013.07.011

Çam, G., (2011). Friction stir welded structural materials: beyond Al-alloys. International Materials Reviews 56(1):1-48. doi: 10.1179/095066010X12777205875750

Dinaharan, I., Murugan, N., (2012a). Optimization of friction stir welding process to maximize tensile strength of AA6061/ZrB$_2$ in-situ composite butt joints. Metals and Materials International 18:135-142. doi: 10.1007/s12540-012-0016-z

Dinaharan, I., Murugan, N., (2012b). Effect of friction stir welding on microstructure, mechanical and wear properties of AA6061/ZrB$_2$ in situ cast composites. Materials Science & Engineering: A 543:257-266. doi: 10.1016/j.msea.2012.02.085

Elangovan, K., Balasubramanian, V., Valliappan, M., (2008). Effect of Tool Pin Profile and Tool Rotational Speed on Mechanical Properties of Friction Stir Welded AA6061 Aluminium Alloy. Materials and Manufacturing Processes 23:251-260. doi: 10.1080/10426910701860723

El-Sabbagh, A. M., Soliman, M., Taha, M. A., Palkowski, H., (2013). Effect of rolling and heat treatment on tensile behaviour of wrought Al-SiCp composites prepared by stir-casting. Journal of Materials Processing Technology 213:1669-1681. doi: 10.1016/j.jmatprotec.2013.04.013

Feng, A. H., Xiao, B. L., Ma, Z. Y., (2008). Effect of microstructural evolution on mechanical properties of friction stir welded AA2009/SiC$_p$ composite. Composites Science and Technology 68:2141-2148. doi: 10.1016/j.compscitech.2008.03.010

Gopalakrishnan, S., Murugan, N., (2011). Prediction of tensile strength of friction stir welded aluminum matrix TiC$_p$ particulate reinforced composite. Materials & Design 32:462- 467. doi: 10.1016/j.matdes.2010.05.055

Guo, J., Gougeon, P., Chen, X. G., (2012). Microstructure evoluation and mechanical properties of dissimilar friction stir welded joints between AA1100-B$_4$C MMC and AA6063 alloy. Materials Science & Engineering: A 553:149-156. doi: 10.1016/j.msea.2012.06.004

Guo, N., Fu, Y., Wang, Y., Meng, Q., Zhu, Y., (2017). Microstructure and mechanical properties in friction stir welded 5A06 aluminum alloy thick plate. Materials & Design 113:273-283. doi: 10.1016/j.matdes.2016.10.030

Ilangovan, M., Boopathy, S. R., Balasubramanian, V., (2015). Effect of tool pin profile on microstructure and tensile properties of friction stir welded dissimilar AA 6061-AA 5086 aluminum alloy joints. Defence Technology 11:174-184. doi: 10.1016/j.dt.2015.01.004

İpekoğlu, G., Çam, G., (2014). Effects of initial temper condition and postweld heat treatment on the properties of dissimilar friction-stir-welded joints between AA7075 and AA6061 aluminum alloys. Metallurgical and Materials Transactions A 45A:3074-3087. doi: 10.1007/s11661-014-2248-7

Kalaiselvan, K., Dinaharan, I., Murugan, N., (2014). Characterization of friction stir welded boron carbide particulate reinforced AA6061 aluminum alloy stir cast composite. Materials & Design 55:176-182. doi: 10.1016/j.matdes.2013.09.067

Kaw, A. K. (2006). Mechanics of Composite Materials. Second Ed. United States of America: Taylor & Francis Group, LLC.

Knowles, A. J., Jiang, X., Galano, M., Audebert, F., (2014). Microstructure and mechanical properties of 6061 Al alloy based composites with SiC nanoparticles. Journal of Alloys and Compounds 615:S401-S405. doi: 10.1016/j.jallcom.2014.01.134

Kovacevic, I., Djelosevic, M., Tepic, G., Milisavljevic, S., (2016). Influential Parameters and Numerical Simulation of Heat Generated in the Process of Friction Stir Welding. Materials Science (MEDŽIAGOTYRA) 22(3):348-353. http://dx.doi.org/10.5755/j01.ms.22.3.10022

Kumar, P. V., Reddy, G. M., Rao, K. S., (2015). Microstructure, mechanical and corrosion behavior of high strength AA7075 aluminium alloy friction stir welds – Effect of post weld heat treatment. Defence Technology 11:362-369. doi: 10.1016/j.dt.2015.04.003

Lee, W-B., Lee, C-Y., Kim, M-K., Yoon, J-I., Kim, Y-J., Yoen, Y-M., Jung, S-B., (2006). Microstructures and wear property of friciton stir welded AZ91 Mg/SiC particle reinforced composite. Composites Science and Technology 66:1513-1520. doi: 10.1016/j.compscitech.2005.11.023

Marzoli, L. M., Strombeck, A. V., Dos Santos, J. F., Gambaro, C., Volpone, L. M., (2006). Friction stir welding of an AA6061/Al$_2$O$_3$/20p reinforced alloy. Composites Science and Technology 66:363-371. doi: 10.1016/j.compscitech.2005.04.048

Narimani, M., Lotfi, B., Sadeghian, Z., (2016). Investigating the microstructure and mechanical properties of Al-TiB$_2$ composite fabricated by Friction Stir Processing (FSP). Materials Science & Engineering: A 673:436-442. doi: 10.1016/j.msea.2016.07.086

Nikoo, M. F., Azizi, H., Parvin, N., Naghibi, H. Y., (2016). The influence of heat treatment on microstructure and wear properties of friction stir welded AA6061-T6/Al$_2$O$_3$ nanocomposite joint at four different traveling speed. Journal of Manufacturing Processes 22:90-98. doi: 10.1016/j.jmapro.2016.01.003

Pantelis, D. I., Karakizis, P. N., Daniolos, N. M., Charitidis, C. A., Koumoulos, E. P., Dragatogiannis, D. A., (2016). Microstructural Study and Mechanical Properties of Dissimilar Friction Stir Welded AA5083-H111 and AA6082-T6 Reinforced with SiC Nanoparticles. Materials and Manufacturing Processes 31:264-274. doi: 10.1080/10426914.2015.1019095

Pirondi, A., Collini, L., Fersini, D., (2008). Fracture and fatigue crack growth behaviour of PMMC friction stir welded butt joints. Engineering Fracture Mechanics 75:4333-4342. doi: 10.1016/j.engfracmech.2008.05.001

Prado, R. A., Murr, L. E., Soto, K. F., McClure, J. C., (2003). Self-optimization in tool wear for friction-stir welding of Al 6061+20% Al$_2$O$_3$ MMC. Materials Science & Engineering: A 349:156-165. doi: 10.1016/S0921-5093(02)00750-5

Prater, T., Strauss, A., Cook, G., Gibson, B., Cox, C., (2013). A comparative evaluation of the wear resistance of various tool materials in friction stir welding of metal matrix composites. Journal of Materials Engineering and Performance 22:1807-1813. doi: 10.1007/s11665-012-0468-9

Root, J. M., Field, D. P., Nelson, T. W., (2009). Crystallographic texture in the friction-stir welded metal matrix composite Al6061 with 10 vol pct Al$_2$O$_3$. Metallurgical and Materials Transactions A 40A:2109-2114. doi: 10.1007/s11661-009-9883-4

Sahraeinejad, S., Izadi, H., Haghshenas, M., Gerlich, A. P., (2015). Fabrication of metal matrix composites by friction stir processing with different particles and processing parameters. Materials Science & Engineering: A 626:505-513. doi: 10.1016/j.msea.2014.12.077

Salih, O. S., Ou, H., Sun, W., McCartney, D. G., (2015). A review of friction stir welding of aluminium matrix composites. Materials & Design 86:67-71. doi: 10.1016/j.matdes.2015.07.071

Schmidt, H., Hattel, J., Wert, J., (2004). An analytical model for the heat generation in friction stir welding. Modelling and Simulation in Materials Science And Engineering 12:143-157. doi: 10.1088/0965-0393/12/1/013

Serindag, H.T., Kiral, B.G., (2017). Friction Stir Welding of AZ31 Magnesium Alloys – A Numerical and Experimental Study. Latin American Journal of Solids and Structures 14:113-130. http://dx.doi.org/10.1590/1679-78253162

Shah, K., (2016). Metal Matrix Composites: The Global Market, Reported by BCC Research. http://www.bccresearch.com/market-research/advanced-materials/metal-matrix-composites-market-report-avm012e.html. Accessed 28 July 2017

Sharifitabar, M., Nami, H., (2011). Microstructures of dissimilar friction stir welded joints between 2024-T4 aluminum alloy and Al/Mg$_2$Si metal matrix cast composite. Composites: Part B 42:2004-2012. doi: 10.1016/j.compositesb.2011.05.025

SupremEX 620XF, (2016). Reported by MATERION. https://materion.com/-/media/files/pdfs/aerospace-metal-composites/supremex/amc620xf-data-sheet-8-15.pdf. Accessed 08 August 2017

Tabasi, M., Farahani, M., Givi, M. K. B., Farzami, M., Moharami, A., (2016). Dissimilar friction stir welding of 7075 aluminum alloy to AZ31 magnesium alloy using SiC nanoparticles. International Journal of Advanced Manufacturing Technology 86:705-715. doi: 10.1007/s00170-015-8211-y

Wang, D., Xiao, B. L., Wang, Q. Z., Ma, Z. Y., (2013). Friction stir welding of SiC$_p$/2009Al composite plate. Materials & Design 47:243-247. doi: 10.1016/j.matdes.2012.11.052